## Measurement of the Coherent Elastic Neutrino-Nucleus Scattering Cross Section on CsI by COHERENT

D. Akimov, P. An, P. An, P. S. Barbeau, P. S. Barbeau, B. Becker, V. Belov, I. Bernardi, M. A. Blackston, C. Bock, A. Bolozdynya, J. Browning, B. Cabrera-Palmer, D. Chernyak, E. Conley, J. Daughhetee, J. Detwiler, M. R. Dirand, P. Efremenko, S. R. Elliott, L. Fabris, M. Febbraro, A. Gallo Rosso, A. Gallo Rosso, A. Galindo-Uribarri, M. P. Green, M. R. Heath, S. Hedges, D. Hoang, M. Hughes, H. T. Johnson, A. Khromov, A. Konovalov, M. P. Green, A. Kumpan, L. Li, J. M. Link, J. Liu, K. Mann, D. M. Markoff, J. Mastroberti, P. E. Mueller, J. Newby, D. S. Parno, S. I. Penttila, D. Pershey, R. Rapp, H. Ray, H. Ray, L. Raybern, O. Razuvaeva, J. D. Reyna, G. C. Rich, J. Ross, D. Rudik, J. Runge, J. D. J. Salvat, A. M. Salyapongse, K. Scholberg, A. Shakirov, G. Simakov, J. G. Sinev, M. M. Snow, M. Snow, M. Sosnovstsev, B. Suh, R. Tayloe, K. Tellez-Giron-Flores, L. Tolstukhin, L. Li, and J. Vanderwerp, A. L. Varner, C. J. Virtue, C. J. Virtue, C. Visser, M. T. Wongjirad, N. Y.-R. Yen, J. Yoo, D. C.-H. Yu, and J. Zettlemoyer, L. Wongjirad, R. Y.-R. Yen, J. J. Yoo, D. C.-H. Yu, and J. Zettlemoyer, A. Statlemoyer, D. S. L. Yen, A. Salvan, J. Zettlemoyer, J. R. Ven, J. J. Yoo, L. Yen, J. Yoo, L. Yu, and J. Zettlemoyer, J. R. Ven, J. J. Yoo, M. Y.-R. Yen, J. Yoo, L. Yu, and J. Zettlemoyer, J. R. Yen, J. Yoo, J. Yoo, J. Yoo, J. Yu, and J. Zettlemoyer, J. R. Yen, J. Yoo, J. Yoo, J. Yoo, J. Yu, A. Yen, J. Yoo, J. Yu, and J. Zettlemoyer, J. Yu, J. Zettlemoyer, J. Yen, J. Yoo, J. Yoo, J. Yoo, J. Yu, A. Yen, J. Yoo, J. Yoo, J. Yu, A. Yen, J. Yu, A. Yen, J. Yu, A. Yen, J. Yu, A. Yen, J. Yoo, J. Yu, A. Yen, J. Yoo, J. Yu, A. Yen, J. Yu, A. Yu, A.

## (COHERENT Collaboration)

<sup>7</sup>Physics Department, University of South Dakota, Vermillion, South Dakota 57069, USA

<sup>8</sup>Department of Physics, North Carolina State University, Raleigh, North Carolina 27695, USA

<sup>9</sup>Sandia National Laboratories, Livermore, California 94550, USA

<sup>10</sup>Center for Experimental Nuclear Physics and Astrophysics, Department of Physics, University of Washington, Seattle, Washington 98195, USA

Los Alamos National Laboratory, Los Alamos, New Mexico 87545, USA
 Department of Physics, Laurentian University, Sudbury, Ontario P3E 2C6, Canada
 Department of Physics, Carnegie Mellon University, Pittsburgh, Pennsylvania 15213, USA
 Department of Physics, Indiana University, Bloomington, Indiana 47405, USA
 Center for Neutrino Physics, Virginia Tech, Blacksburg, Virginia 24061, USA
 Department of Mathematics and Physics, North Carolina Central University,
 Durham, North Carolina 27707, USA

<sup>17</sup>Department of Physics, University of Florida, Gainesville, Florida 32611, USA
 <sup>18</sup>Department of Physics and Astronomy, Tufts University, Medford, Massachusetts 02155, USA
 <sup>19</sup>Department of Physics and Astronomy, Seoul National University, Seoul 08826, Korea

(Received 2 June 2022; revised 17 July 2022; accepted 3 August 2022; published 17 August 2022)

We measured the cross section of coherent elastic neutrino-nucleus scattering (CEvNS) using a CsI[Na] scintillating crystal in a high flux of neutrinos produced at the Spallation Neutron Source at Oak Ridge National Laboratory. New data collected before detector decommissioning have more than doubled the dataset since the first observation of CEvNS, achieved with this detector. Systematic uncertainties have also been reduced with an updated quenching model, allowing for improved precision. With these analysis improvements, the COHERENT Collaboration determined the cross section to be  $(165^{+30}_{-25}) \times 10^{-40}$  cm<sup>2</sup>, consistent with the standard model, giving the most precise measurement of CEvNS yet. The timing structure of the neutrino beam has been exploited to compare the CEvNS cross section from scattering of

Published by the American Physical Society under the terms of the Creative Commons Attribution 4.0 International license. Further distribution of this work must maintain attribution to the author(s) and the published article's title, journal citation, and DOI. Funded by SCOAP<sup>3</sup>.

different neutrino flavors. This result places leading constraints on neutrino nonstandard interactions while testing lepton flavor universality and measures the weak mixing angle as  $\sin^2 \theta_W = 0.220^{+0.028}_{-0.026}$  at  $O^2 \approx (50 \text{ MeV})^2$ .

DOI: 10.1103/PhysRevLett.129.081801

Introduction.—Coherent elastic neutrino-nucleus scattering (CEvNS) is a neutral-current process [1,2] with low momentum transfer  $Q^2$ , where the neutrino interacts coherently with the nucleus. The recoil energy transferred to the nucleus is observable, though typical recoil energies are low, tens of keV for neutrino energies in the tens of MeV range. Thus, detectors with low-energy thresholds are required for CEvNS measurement.

CEvNS has the largest cross section among neutrino scattering channels for neutrino energies below 100 MeV for most target nuclei. The standard model (SM) prediction depends on the nuclear weak charge,  $Q_W^2 = [N - (1 - 4\sin^2\theta_W)Z]^2 \approx N^2$ , where N and Z are the neutron and proton numbers of the target nucleus, and  $\theta_W$  is the weak mixing angle [3]. CEvNS was first measured using the COHERENT CsI[Na] detector in an intense, pulsed source of neutrinos produced at the Spallation Neutron Source (SNS) [4,5] at Oak Ridge National Laboratory [6].

The COHERENT experiment deploys several detectors designed to measure CEvNS and other low-energy scattering processes using the  $\pi^+$  decay-at-rest ( $\pi DAR$ ) neutrino flux at the SNS, attractive for CEvNS measurements [7]. The detectors are situated in "neutrino alley" (NA), a basement hallway where background neutrons from the facility are heavily suppressed. CEvNS was first observed in NA, 19.3 m from the neutrino source using a 14.6 kg CsI [Na] scintillating detector [6] 43 yr after its theoretical prediction [1]. COHERENT also made the first detection of CEvNS on argon [8], which, together with the initial CsI [Na] measurement, agrees with the  $N^2$  scaling of the cross section. While these campaigns were highly successful, they suffer from large statistical and systematic uncertainties, which limit their sensitivity to searches for new physical phenomena.

CEvNS is a precisely predicted neutrino interaction within the SM. The theoretical uncertainty is dominated by understanding of the spatial distribution of the weak charge in the nucleus. As a result, CEvNS is a process well suited for probing physics beyond the SM (BSM). A precision measurement of CEvNS is sensitive to new particles, such as a dark photon that interferes with Z exchange in the low- $Q^2$  regime [9–11] and may explain the g-2 anomaly [12]. Similarly, through the reliance of  $Q_W^2$  on  $\sin^2\theta_W$ , CEvNS may identify new physics through an unexpected value of the effective weak mixing angle at  $Q^2\approx(50 \text{ MeV})^2$  [11]. It can shed light on new forces at high mass scales through nonstandard interaction (NSI) searches [13]. Further, CEvNS measurements are crucial

for interpreting neutrino oscillation measurements, as oscillation experiments alone cannot distinguish between the large mixing angle (LMA) and LMA-dark mixing parameters. Scattering experiments are needed to lift this degeneracy, and future COHERENT data may soon eliminate this ambiguity completely [14–16].

Detectors that measure CEvNS are also sensitive to sub-GeV, accelerator-produced dark matter particles [17,18]. Further, CEvNS from solar and atmospheric neutrinos is a background for dark matter direct detection experiments [19–21], making up the so-called neutrino floor, so that a clear understanding of their interaction will soon become paramount.

CEvNS will also contribute to measuring a future supernova neutrino burst [22,23]. As a neutral-current process, CEvNS is sensitive to the total neutrino flux, which is of particular interest, as other detection channels are most sensitive to the  $\nu_e$  [24] or  $\bar{\nu}_e$  [25] flux. CEvNS is also understood to play an important role in energy transport driving the core-collapse mechanism in the supernova [26–29].

In this Letter, we present the first such measurement with the final CsI[Na] dataset and improved understanding of systematic uncertainties. Using the time structure of the neutrino flux from  $\pi DAR$ , leading constraints on non-standard neutrino interactions are presented, along with a direct measurement of the weak mixing angle at low  $Q^2$ .

Experiment.—We used the 14.6-kg scintillation CsI[Na] crystal, which made the first observation of CEvNS [6] with an identical shielding and hardware configuration. The crystal's dopant was selected to reduce the rate of afterglow scintillation following a burst of activity in the detector [30]. The crystal was attached to a single Hamamatsu R877-100 photomultiplier tube (PMT). The signal was digitized at a rate of 500 MS/s with a dynamic range extending beyond the  $60\text{-keV}_{ee}$  calibration scale. This crystal was shielded with both low-activity lead and low-Z materials to mitigate  $\gamma$  and neutron backgrounds [30,31]. Muon veto panels surrounded the detector, which allowed for removal of cosmic-associated activity.

Our dataset includes 13.99 GWh of integrated beam power that passes live time criteria on beam stability, detector condition, and afterglow rate. During data collection, the SNS ran using a mercury target with a mean beam energy of 0.984 GeV yielding  $3.20 \times 10^{23}$  protons on target (POT). The beam was pulsed at 60 Hz with a 378-ns wide (FWHM) time profile and a 6- $\mu$ s CEvNS timing window per spill. Averaged over beam energies, a pion yield of

 $0.0848 \pm 10\% \, \pi^+/\text{POT}$  is expected from a GEANT4 [32] simulation of the SNS beam [33]. The POT timing distribution averaged over the running period is calculated using beam current data from the SNS and has a FWHM of 378 ns. Since this is less than the muon lifetime, the flux separates into two populations: a prompt, predominantly  $\nu_{\mu}$  flux from  $\pi^+$  decay followed by a delayed flux of  $\nu_e$  and  $\bar{\nu}_{\mu}$  from subsequent  $\mu^+$  decay. Over 99% of the SNS neutrino flux is generated by  $\pi^+$  decay at rest [33].

The detector was calibrated with the 59.5-keV  $\gamma$  decay of an <sup>241</sup>Am source. With a Gaussian fit to calibration data, we found a light yield of 13.35 photoelectrons per keV electron equivalent (PE/keV<sub>ee</sub>). Calibration data were taken with the source at nine different locations along the crystal, finding a spatial spread in light yield less than 3%. The single PE (SPE) charge was monitored during SNS running by tagging single PMT pulses with little other activity in the crystal.

Data analysis.—Our analysis procedure closely parallels the approach described in [6,34] with improvements to our simulation, reoptimization of our event selection, and a more thorough detector response model. Data coincident with the arrival of the beam were blinded until reconstruction, selection, and analysis methods were determined. Event time and energy were reconstructed by analyzing the PMT waveform in the beam window.

The PMT voltage traces were digitized and a 70- $\mu$ s waveform was saved for every beam spill. We formed a 15- $\mu$ s region of interest (ROI) coincident with the arrival of the beam and formed a 3- $\mu$ s integration time to capture most light given by a dominant scintillation decay constant,  $\tau = 0.6 \ \mu$ s [30]. The CsI[Na] crystal used also exhibits a low rate of afterglow scintillation up to 1 ms following a prompt energy deposit. We monitored for afterglow by analyzing a 40- $\mu$ s pretrace region (PTR) immediately preceding the ROI to measure the afterglow rate on a spill-by-spill basis. We also analyzed an analogous anticoincident (AC) region preceding the beam to monitor steady-state backgrounds (SSBs).

We applied two selection cuts to the waveform PTR. First, backgrounds producing afterglow contamination in the signal ROI are more likely to have more activity in the PTR; we therefore only selected events with five or fewer PTR pulses. A new cut is introduced to remove events that have a pulse within the last 200 ns of the PTR, which are typically background events that scatter very late in the PTR and then leak into the ROI that was not considered in [6].

Only events with  $\geq 9$  pulses reconstructed in the ROI are selected and the energy, measured in PEs, is determined by the waveform integral of reconstructed pulses. This mitigates background from coincidence of afterglow pulses. These events are predicted to be biased to early scattering times, with approximately exponential shape,  $\tau \approx 4 \ \mu s$ . Using this time dependence, we validated this simulation

by comparing the rate and time dependence of the afterglow background using AC data and confirm that a negligible afterglow rate, consistent with zero, is expected after the  $\geq 9$  pulse cut. This restriction was made stronger than that used for the initial CEvNS measurement [6] after the identification of this background, as the exponential shape of the afterglow could bias the estimated CEvNS content at early times by  $\approx 14\%$ , which could imitate a signature of new physics such as dark matter in the dataset.

We applied nuclear recoil quenching by fitting the scintillation response curve  $E_{ee} = f(E_{\rm nr})$  to five datasets collected in CsI[Na], including three taken by COHERENT [35,36]. The quenching model used is discussed in detail in [35]. The recoil energies in the quenching datasets spanned from 3 to 63 keV<sub>ee</sub>. To account for shape as a function of  $E_{\rm nr}$ , we parametrized the scintillation response curve as a fourth degree polynomial, constrained so that f(0) = 0.

The selection efficiency for CEvNS recoils depends on observed energy, PEs, and recoil time  $t_{\rm rec}$ . We estimated energy dependence of the efficiency and its uncertainty using <sup>133</sup>Ba calibration data, which gave a sample of Compton-scattered electrons. A coincidence with a backing detector was used to mitigate background and ensure only low-energy forward scattering events were used in the calibration.

There is a 39% chance that there is at least one afterglow pulse in each waveform ROI. Since we reconstructed  $t_{rec}$  as the time of the first pulse in the ROI, it is possible for a CEvNS recoil occurring at late  $t_{rec}$  to be rejected because it follows a random pulse, which is accounted for in a timedependent efficiency  $\varepsilon_T$ . Previously,  $\varepsilon_T$  was assumed to be one [6], but we have now estimated with a data-driven simulation. A library of waveforms from AC data was constructed. A simulated CEvNS waveform was then overlaid on a waveform randomly selected from this library. We took  $\varepsilon_T$  as the ratio of events selected when simulated at  $t = t_{\rm rec}$  compared to t = 0. We also expect signal events that follow a random afterglow pulse but within the 3  $\mu$ s integration window. These events may be selected, but would have biased recoil energy and time. This background was mitigated by requiring the time difference between the first and second pulse in the ROI to be < 520 ns. This cut rejected < 1% of properly reconstructed events, but reduced the fraction of biased events to 2% of the sample. This was validated with large PE inelastic signals in our detector, whose onset time was unambiguous.

Our energy resolution was dominated by photon counting. However, variations in the SPE charge were also included as the standard deviation of the SPE distribution was  $\approx 50\%$  the mean value. This added an additional smearing of  $50\%/\sqrt{N_{\rm pulse}}$ . A 3% broadening is also included due to potential spatial nonuniformity of the light yield. Combining these effects, the smearing was modeled with a gamma function, which predicts the asymmetric

simulated distribution as detailed in the Supplemental Material [37].

Over 98% of the background comes from beam-uncorrelated SSB. This background is measured *in situ* from AC data. We estimated the PE distribution using all events found in AC data and used an exponential model for the time distribution with  $\tau = 20.2 \pm 2.6 \,\mu s$ , consistent with the time dependence of the signal efficiency. Uncertainty in this decay constant had < 0.5% impact on the measured cross section and was neglected.

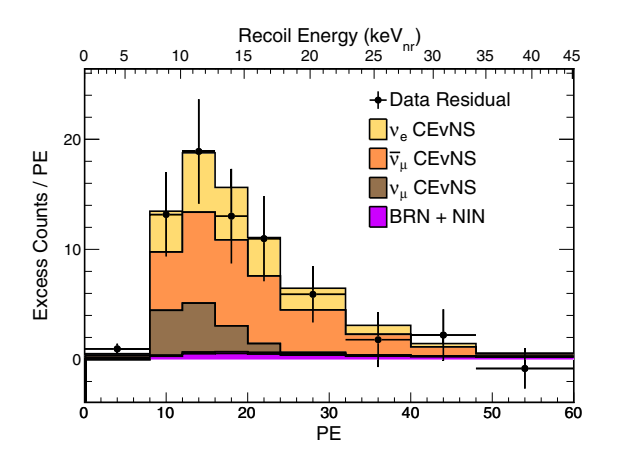
We accounted for two sources of beam-related background: beam-related neutron (BRN) and neutrino-induced neutron (NIN) scatters. Prior to detector installation, the normalization of each of these components was studied by an EJ-301 liquid scintillator detector [38] housed in the CsI [Na] shielding. The neutron-moderating water used in the detector shielding was drained to increase the neutron rate. The BRN and NIN timing distributions are different: BRN events are prompt, while NIN events follow the neutrino timing distribution. The BRN and NIN rates, therefore, were determined from a fit to the time distribution [6]. A MCNPX-PoliMi [39] simulation was used to estimate the total flux of neutrons from each source incident on the EJ-301 detector. This flux was then propagated through the full shielding into the CsI[Na] detector to simulate the neutron background. We assume a power-law BRN flux,  $\phi \propto E^{-\alpha}$  with  $\alpha = 1.2$ . Changes in the value of  $\alpha$  had no statistically significant effect on the shape of our background distributions. The NIN spectrum was estimated using MARLEY [40,41] tuned to production on <sup>208</sup>Pb with an incident  $\pi DAR$  spectrum. After selection, we estimated  $18 \pm 25\%$  BRN and  $6 \pm 35\%$  NIN events in our sample with uncertainty dominated by the statistical precision of the EJ-301 fit [6]. Together BRN and NIN backgrounds are small, about 7% of the predicted CEvNS rate.

We performed a binned likelihood fit to data in both PE and  $t_{\rm rec}$ . All data events with PE < 60 and  $t_{\rm rec}$  < 6  $\mu$ s were included in the fit. Systematic uncertainties were

included as nuisance parameters, including shape effects. Uncertainty parameters were profiled in the fit. We accounted for normalization uncertainty on each component. The CEvNS uncertainty is 10%, dominated by the understanding of the total neutrino flux [33]. We also included a 2.1% uncertainty on the SSB normalization due to a finite sample used to estimate the background.

We also fit five systematic parameters that affect the shape of our predicted spectra. The timing onset of the neutrino flux through our detector was allowed to float without any prior constraint. Uncertainty in quenching was calculated by a principal component analysis (PCA) of the covariance matrix from fit to available data. We identified two impactful uncertainties from the PCA, giving a combined 3.8% bias in our fit. A PCA was also performed on our CEvNS efficiency curve from <sup>133</sup>Ba calibration data. This resulted in one systematic parameter that is roughly equivalent to a 1.0 PE uncertainty in threshold and gives a 4.1% uncertainty. Finally, our form-factor uncertainty adjusts the neutron radius in CsI  $R_n$  by  $\pm 5\%$ , which shifts the theoretical CEvNS cross section by 3.4% and gives a 0.6% uncertainty on our measured cross section. Nonzero values of NSI parameters would modify the relative vector and axial contributions to the CEvNS cross section, which would affect form-factor suppression [42], but this effect has a < 0.1% impact on constraints in CsI and is dropped.

*Results.*—After fitting, we observed  $306 \pm 20$  CEvNS events, consistent with the SM prediction of  $341 \pm 11$  (theory)  $\pm 42$ (experiment). The best-fit residual CEvNS spectra in PE and  $t_{\rm rec}$  are shown in Fig. 1. The best-fit prediction models the observed data well with a  $\chi^2$ /degrees of freedom = 82.6/98. No excess is observed in beam-off data. The cross section averaged over the  $\nu_{\mu}/\nu_{e}/\bar{\nu}_{\mu}$  flux  $\langle \sigma \rangle_{\Phi}$  was determined to be  $(165^{+30}_{-25}) \times 10^{-40}$  cm<sup>2</sup> by a profiled log-likelihood fit. This is consistent with the SM prediction of  $(189 \pm 6) \times 10^{-40}$  cm<sup>2</sup>. The observed data reject the no-CEvNS hypothesis at  $11.6\sigma$ . See the Supplemental Material [37] to see observed data



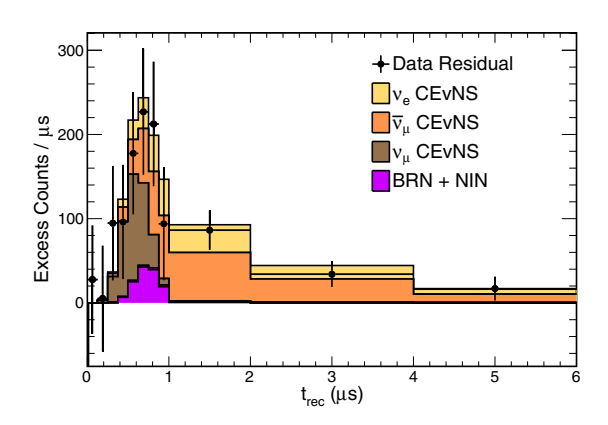


FIG. 1. The data residual over SSB compared to best-fit CEvNS, BRN, and NIN predictions projected onto the PE (left) and  $t_{rec}$  (right) axes. The CEvNS distribution has been decomposed into each flavor of neutrino flux at the SNS.

listed along with assumptions required to reproduce this result.

Since the SM cross section depends on the weak charge, the CEvNS cross section can be interpreted as a constraint on the weak mixing angle at a low momentum exchange  $Q^2 \approx (50 \text{ MeV})^2$ , consistent with previous results [43]. Our current result implies  $\sin^2 \theta_W = 0.220^{+0.028}_{-0.026}$  compared to the SM prediction 0.23857(5) [44]. Current constraints at low  $Q^2$  from atomic parity violation measurements are much more precise, though a percent-level measurement from COHERENT will be possible within the future [45]. Additionally, as  $^{133}$ Cs is a commonly used atom for these studies [46,47], CEvNS data can be used to constrain theoretical uncertainties on nuclear structure assumed in these results [3].

The "flavored" CEvNS cross sections  $\langle \sigma \rangle_{\mu}$  and  $\langle \sigma \rangle_{e}$  are also measured by exploiting the differences in timing shapes between the CEvNS contributions from  $\nu_{\mu}$ ,  $\bar{\nu}_{\mu}$ , and  $\nu_{e}$ . This parameter space is a sensitive probe of BSM physics such as neutrino-quark vector NSIs, which can affect each neutrino flavor differently [13]. The flavored CEvNS cross section result is uniquely possible using a flux from a spallation source with beam width less than the muon half-life. The allowed contour in this parameter space is shown in Fig. 2. The best-fit scales relative to the SM are 0.88 and 0.87 for  $\langle \sigma \rangle_{\mu}$  and  $\langle \sigma \rangle_{e}$ , respectively, consistent with the SM within uncertainties.

We used this measurement to constrain heavy-mediator  $(m_V \gg Q)$  neutrino-quark NSIs, commonly parameterized as a matrix of  $\varepsilon_{ij}^f$  where  $i, j = e, \mu, \tau$  and f = u, d. Existence of NSIs could confuse ongoing efforts to measure the neutrino mixing matrix parameters. Notably,

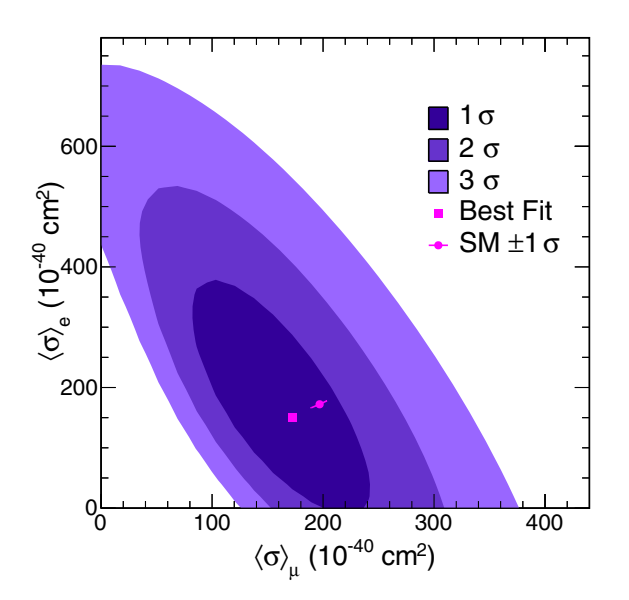


FIG. 2. Contours for the flavored CEvNS cross section. The best-fit parameters and the SM prediction, along with  $\pm 1~\sigma$  error bands from form-factor uncertainty, are shown as pink markers.

it is possible to reverse the inferred neutrino mass ordering from oscillation data by choosing a suitable set of NSI parameters [14]. Also, NSIs allow for additional CP-violating phases, which may bias constraints on  $\delta_{CP}$  [15,48].

In Fig. 3, we show the constraint on  $\varepsilon_{ee}^u$  and  $\varepsilon_{ee}^d$  with other parameters fixed to zero compared to CHARM [49] constraints. This marks a significant improvement over the previous CsI[Na] constraint from COHERENT [6] because of an improved precision result and measuring the flavored cross sections. There are also NSI constraints determined from CEvNS data on Ar [8] and Xe [50], though these limits are currently less precise.

Figure 3 also shows our sensitivity to  $\varepsilon_{ee}^{u}$  and  $\varepsilon_{\mu\mu}^{u}$ . This combination is directly related to solar neutrino oscillation results. In the context of NSIs, there is a degeneracy in

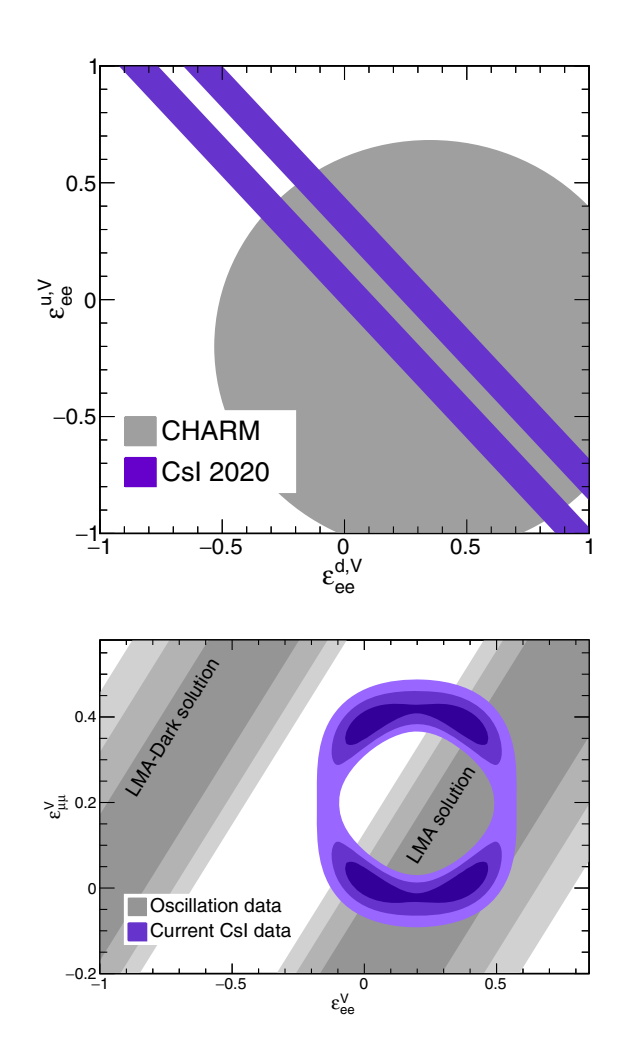


FIG. 3. Top: the 90% allowed parameter space with  $\varepsilon^u_{ee}$  and  $\varepsilon^d_{ee}$  allowed to float while fixing others at zero. Bottom: the  $1/2/3\sigma$  contours allowing  $\varepsilon^u_{ee}$  and  $\varepsilon^u_{\mu\mu}$  to float, fixing others to zero. The bottom also shows parameter space that is compatible with a degeneracy in solar neutrino oscillation data that would flip the inferred neutrino mass ordering.

oscillation data between the LMA and LMA-dark solutions that differ in the  $\theta_{12}$  octant and altering the interpretation of the neutrino mass ordering [51]. The shape of the allowed parameter space again highlights the power of the flavored CEvNS measurement, as  $\varepsilon_{ee}^{u,V}$  and  $\varepsilon_{\mu\mu}^{u,V}$  only affect the CEvNS cross section for  $\nu_e$ - and  $\nu_\mu$ -flavor neutrinos, respectively.

Conclusion.—We measured the CEvNS cross section using the full dataset collected by the CsI[Na] scintillation detector using a blinded analysis approach. With doubled exposure and improved understanding of systematic uncertainties, we have made the most precise measurement of CEvNS to date, observing CEvNS at  $11.6\sigma$  and finding a flux-averaged cross section  $\langle \sigma \rangle_{\Phi} = (165^{+30}_{-25}) \times 10^{-40}$  cm<sup>2</sup>, consistent with the SM prediction to within  $1\sigma$ . The weak mixing angle was measured at low  $Q^2$ . We also introduced measurements of the flavored CEvNS cross section, which improve CEvNS constraints on neutrino-quark NSI scenarios. Though the CsI[Na] detector has been decommissioned, a planned calibration of the neutrino flux using a heavy-water Cherenkov detector [52] will further improve precision of the CEvNS measurements. COHERENT is currently engaged in ongoing measurements of CEvNS on Ar, Ge, and NaI, while additional targets are possible for the future.

The COHERENT Collaboration acknowledges the Kavli Institute at the University of Chicago for CsI[Na] detector contributions. The COHERENT Collaboration acknowledges the generous resources provided by the ORNL Spallation Neutron Source, a DOE Office of Science User Facility, and thanks Fermilab for the continuing loan of the CENNS-10 detector. We also acknowledge support from the Alfred P. Sloan Foundation, Consortium for Nonproliferation Enabling Capabilities, National Science Foundation, Russian Foundation for Basic Research (Project No. 17-02-01077 A), Korea National Research Foundation (NRF 2022R1A3B1078756), and U.S. Department of Energy, Office of Science. Laboratory directed research and development funds from ORNL and Lawrence Livermore National Laboratory also supported this project. This research used the Oak Ridge Leadership Computing Facility, which is a DOE Office of Science User Facility. Sandia National Laboratories is a multimission laboratory managed and operated by National Technology and Engineering Solutions of Sandia, LLC, a wholly owned subsidiary of Honeywell International, Inc., for the U.S. Department of Energy's National Nuclear Security Administration under Award No. DE-NA0003525. The work was supported by the Ministry of Science and Higher Education of the Russian Federation, Project Fundamental Properties of Elementary Particles and Cosmology No. 0723-2020-0041.

- \*Present address: Institute for Nuclear Research of NASU, Kyiv 03028, Ukraine.
- <sup>†</sup>Present address: South Dakota School of Mines and Technology, Rapid City, South Dakota 57701, USA.
- <sup>‡</sup>Present address: Argonne National Laboratory, Argonne, Illinois 60439, USA.
- <sup>§</sup>Present address: Fermi National Accelerator Laboratory, Batavia, Illinois 60510, USA.
- [1] D. Z. Freedman, Phys. Rev. D 9, 1389 (1974).
- [2] V. Kopeliovich and L. Frankfurt, JETP Lett. 19, 145 (1974), http://jetpletters.ru/ps/1776/article 27044.shtml.
- [3] M. Cadeddu and F. Dordei, Phys. Rev. D 99, 033010 (2019).
- [4] T. E. Mason, T. A. Gabriel, R. K. Crawford, K. W. Herwig, F. Klose, and J. F. Ankner, eConf C000821, FR203 (2000), https://www.slac.stanford.edu/econf/C000821/FR203.shtml.
- [5] R. L. Kustom, eConf C000821, TU101 (2000), https://www.slac.stanford.edu/econf/C000821/TU101.shtml.
- [6] D. Akimov *et al.* (COHERENT Collaboration), Science **357**, 1123 (2017).
- [7] K. Scholberg, Phys. Rev. D 73, 033005 (2006).
- [8] D. Akimov *et al.* (COHERENT Collaboration), Phys. Rev. Lett. **126**, 012002 (2021).
- [9] H. Davoudiasl, H.-S. Lee, and W. J. Marciano, Phys. Rev. D 89, 095006 (2014).
- [10] J. Liao and D. Marfatia, Phys. Lett. B 775, 54 (2017).
- [11] O. Miranda, D. Papoulias, G. Sanchez Garcia, O. Sanders, M. Tórtola, and J. Valle, J. High Energy Phys. 05 (2020) 130.
- [12] B. Abi *et al.* (Muon *g* 2 Collaboration), Phys. Rev. Lett. **126**, 141801 (2021).
- [13] J. Barranco, O. Miranda, and T. Rashba, J. High Energy Phys. 12 (2005) 021.
- [14] P. Coloma, I. Esteban, M. Gonzalez-Garcia, and M. Maltoni, J. High Energy Phys. 02 (2020) 023.
- [15] P.B. Denton, J. Gehrlein, and R. Pestes, Phys. Rev. Lett. **126**, 051801 (2021).
- [16] P. B. Denton and J. Gehrlein, Phys. Rev. D **106**, 015022 (2022).
- [17] B. Dutta, S. Liao, S. Sinha, and L. E. Strigari, Phys. Rev. Lett. 123, 061801 (2019).
- [18] D. Akimov *et al.* (COHERENT Collaboration), Phys. Rev. D **102**, 052007 (2020).
- [19] J. Billard, E. Figueroa-Feliciano, and L. Strigari, Phys. Rev. D 89, 023524 (2014).
- [20] C. A. J. O'Hare, Phys. Rev. D 94, 063527 (2016).
- [21] C. Bœhm, D. Cerdeño, P. Machado, A. Olivares-Del Campo, E. Perdomo, and E. Reid, J. Cosmol. Astropart. Phys. 01 (2019) 043.
- [22] C. J. Horowitz, K. J. Coakley, and D. N. McKinsey, Phys. Rev. D 68, 023005 (2003).
- [23] R. F. Lang, C. McCabe, S. Reichard, M. Selvi, and I. Tamborra, Phys. Rev. D 94, 103009 (2016).
- [24] B. Abi et al. (DUNE Collaboration), Eur. Phys. J. C 80, 978 (2020).
- [25] K. Abe *et al.* (Super-Kamiokande Collaboration), Astropart. Phys. **81**, 39 (2016).
- [26] J. R. Wilson, Phys. Rev. Lett. 32, 849 (1974).

- [27] D. N. Schramm and W. D. Arnett, Phys. Rev. Lett. **34**, 113 (1975).
- [28] D. Z. Freedman, D. N. Schramm, and D. L. Tubbs, Annu. Rev. Nucl. Sci. 27, 167 (1977).
- [29] K. Balasi, K. Langanke, and G. Martínez-Pinedo, Prog. Part. Nucl. Phys. 85, 33 (2015).
- [30] J. Collar, N. Fields, M. Hai, T. Hossbach, J. Orrell, C. Overman, G. Perumpilly, and B. Scholz, Nucl. Instrum. Methods Phys. Res., Sect. A 773, 56 (2015).
- [31] N. E. Fields, CosI: Development of a low threshold detector for the observation of coherent elastic neutrino-nucleus scattering, Ph.D. thesis, The University of Chicago, 2014.
- [32] S. Agostinelli et al. (GEANT4 Collaboration), Nucl. Instrum. Methods Phys. Res., Sect. A 506, 250 (2003).
- [33] D. Akimov et al., Phys. Rev. D 106, 032003 (2022).
- [34] B. J. Scholz, First observation of coherent elastic neutrinonucleus scattering, Ph.D. thesis, Chicago University, 2017, arXiv:1904.01155.
- [35] D. Akimov et al. (COHERENT Collaboration), arXiv:2111. 02477.
- [36] J. I. Collar, A. R. L. Kavner, and C. M. Lewis, Phys. Rev. D 100, 033003 (2019).
- [37] See Supplemental Material at http://link.aps.org/supplemental/10.1103/PhysRevLett.129.081801 for selected data, along with specifications for recreating this result.
- [38] Eljen Technology, 1300 W. Broadway Street, Sweetwater, TX 79556.

- [39] S. A. Pozzi, E. Padovani, and M. Marseguerra, Nucl. Instrum. Methods Phys. Res., Sect. A 513, 550 (2003).
- [40] S. Gardiner, Nuclear effects in neutrino detection, Ph.D. thesis, University of California, Davis, 2018.
- [41] S. Gardiner, Phys. Rev. C 103, 044604 (2021).
- [42] M. Hoferichter, J. Menéndez, and A. Schwenk, Phys. Rev. D 102, 074018 (2020).
- [43] D. Androic *et al.* (Q<sub>weak</sub> Collaboration), Phys. Rev. Lett. 111, 141803 (2013).
- [44] P. Zyla et al. (Particle Data Group), Prog. Theor. Exp. Phys. 2020, 083C01 (2020).
- [45] D. Akimov et al., in 2022 Snowmass Summer Study (2022), arXiv:2204.04575.
- [46] C. S. Wood, S. C. Bennett, D. Cho, B. P. Masterson, J. L. Roberts, C. E. Tanner, and C. E. Wieman, Science 275, 1759 (1997).
- [47] V. A. Dzuba, J. C. Berengut, V. V. Flambaum, and B. Roberts, Phys. Rev. Lett. 109, 203003 (2012).
- [48] A. N. Khan, D. W. McKay, and W. Rodejohann, Phys. Rev. D 104, 015019 (2021).
- [49] J. Dorenbosch et al., Phys. Lett. B 180, 303 (1986).
- [50] E. Aprile et al., Phys. Rev. Lett. 126, 091301 (2021).
- [51] P. Coloma, M. C. Gonzalez-Garcia, M. Maltoni, and T. Schwetz, Phys. Rev. D 96, 115007 (2017).
- [52] D. Akimov et al., J. Instrum. 16, P08048 (2021).